d-wave superconductivity, antiferromagnetism and spin liquid in quasi-two-dimensional organic superconductors

P Sahebsara and D Sénéchal

Département de physique and Regroupement québécois sur les matériaux de pointe, Université de Sherbrooke,
Sherbrooke, Québec, Canada, J1K 2R1

Abstract

The self-energy-functional approach is a powerful many-body tool to investigate different broken symmetry phases of strongly correlated electron systems. We use the variational cluster perturbation theory (also called the variational cluster approximation) to investigate the interplay between the antiferromagnetism and d-wave superconductivity of κ-(ET)$_2$ X conductors. These compounds are described by the so-called dimer Hubbard model, with various values of the on-site repulsion U and diagonal hopping amplitude t'. At strong coupling, our zero-temperature calculations show a transition from Néel antiferromagnetism to a spin-liquid phase with no long range order, at around $t' \sim 0.9$. At lower values of U, we find d-wave superconductivity. Taking into account the point group symmetries of the lattice, we find a transition between $d_{x^2-y^2}$ and d_{xy} pairing symmetries, the latter happening for smaller values of U.

1. Introduction

Low-dimensional systems of strongly correlated interacting electrons, such as cuprate and organic compounds, have been vastly studied in recent experimental and theoretical researches. Variation of doping or chemical pressure is often the cause of an antiferromagnetic-superconducting phase transition in these compounds. A subject of great interest has been the proximity of antiferromagnetism (AF) and unconventional superconductivity (SC) and the possible existence of other exotic phases in the κ-family of organic superconductors. The general chemical formula for this family of organic compounds is κ-(BEDT-TTF)$_2$X, where BEDT-TTF is an abbreviation for bisethylenedithio-tetrathiafulvalene, and the anion X can be one of X=Cu(NCS)$_2$, Cu[N(CN)$_2$]Br, Cu$_2$ (CN)$_3$, I$_3$,etc [1,2]. These are basically quasi-bidimensional systems, in which holes are constrained to move mostly in the layer of BEDT-TTF molecules, as shown in Figure 1. The layer of anions plays the role of a barrier to the hole motion. Understanding the electronic properties and the microscopic phase transition in these materials is a great theoretical challenge [3-5,16].

For instance, the compound κ-(BEDT-TTF)$_2$ Cu[N(CN)$_2$]Cl (shortly written as κ-Cl) shows a transition between antiferromagnetism and superconductivity under pressure, with a macroscopic coexistence of the two phases in some range of pressure [7,8]. On the other hand, in κ-(BEDT-TTF)$_2$ Cu$_2$ (CN)$_3$ (or κ–Cu$_2$CN$_3$), a higher level of magnetic frustration leads to a Mott transition upon decreasing pressure without magnetic ordering [9,10].

The focus of this paper are the zero-temperature ordered phases (AF and d-wave SC) of this family of compounds as described by the dimer Hubbard model (defined below). The method used is variational cluster perturbation theory (VCPT), also called the variational cluster approximation (VCA) [11,12]. This method is based on the self-energy functional approach proposed by Potthoff [13], and has been capable of reproducing the AF and dSC phases of high-temperature superconductors [14,15]. It is based on a dynamic variational principle, i.e., involving the frequency-dependent one-body Green function of the system. As such, it provides not only order parameters, but also dynamic information like the spectral function.

2. Properties of the κ-(BEDT-TTF)$_2$ X family

2.1. Lattice structure

The structure of κ-(BEDT-TTF)$_2$ X consists of lattice of pairs (dimers) of aligned molecules (1). A schematic view of the $b-c$ plane is shown on the left panel of figure 2. The BEDT-TTF layers and the anion layers alternate along the a-axis. The presence of the
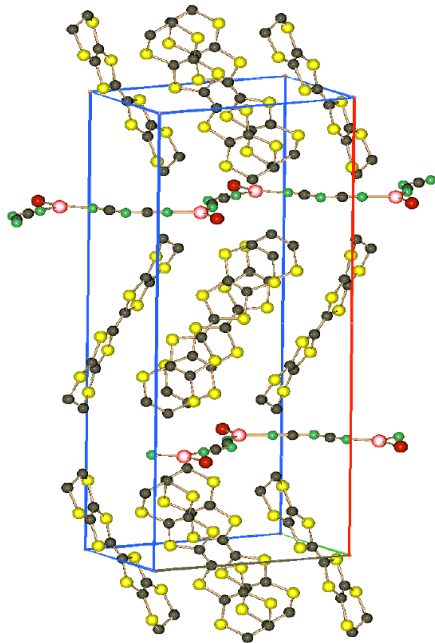
Figure 1. (color online) Crystal structure of κ-(BEDT-TTF)$_2$ X. Each two-dimensional layer of BEDT-TTF molecules is sandwiched between two X anion layers. (Reprinted from ref.[6], Copyright 2001, with permission from Elsevier.)

monovalent anion X introduces a hole (charge carrier) into each dimer, making the antibonding molecular orbital of the dimer half filled. A relatively large overlap of the orbitals between the dimers and the very small overlap between the BEDT-TTF layers, causes the carriers to move preferentially within the BEDT-TTF layers, resulting in a quasi two-dimensional character. The holes can hop through the triangular lattice of dimers to their nearest (NN) and next-nearest (NNN) neighbor, via two inter-dimer transfer integrals, t and t', of the order of 50 meV, as shown in figure 2. These hopping integrals are affected by chemical or hydrostatic pressure.

The relative value of the hopping integrals t and t', which depends on the anion type, determines the degree of magnetic frustration in the system. The case $t' = 0$ would correspond to a square lattice, whereas the case $t' = t$ corresponds to an isotropic triangular lattice. Values of the hopping integrals for four members of the family are given in Table 1.

2.2. Phase diagram
The family κ-BEDT-TTF$_2$X has a very rich phase diagram as a function of pressure, temperature and anion. The resistivity profiles of a few BEDT salts are shown in Figure 3. Note that κ-Cu(NCS)$_2$ and κ-Br are metals (their resistivity decreases with temperature) that turn into superconductors (critical temperatures are indicated in Table I). On the other hand, κ-Cl is an insulator at ambient pressure. So is κ-Cu$_2$CN$_3$ (not shown on figure 3). But these two insulating compounds
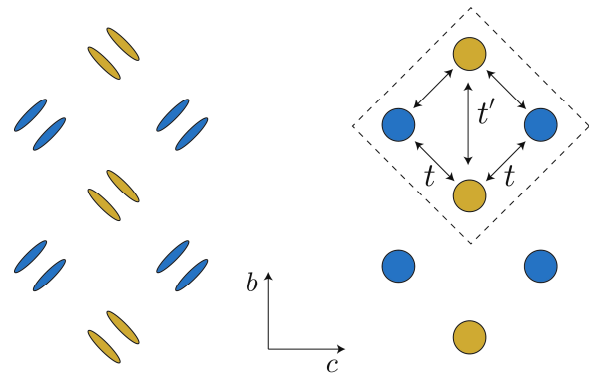
Figure 2. (color ongline) (a) The lattice structure of κ -(BEDT-TTF)$_2$ X in the *b-c* plane. (b) The lattice structure of the dimers of aligned BEDT-TTF molecules. t and t' represent the hopping integrals to nearest and next-nearest neighbor site, respectively. The dashed square represents a 4-site cluster used in the VCA.

differ in that κ-Cl becomes an antiferromagnetic insulator at low temperature [8], whereas κ-Cu$_2$CN$_3$ shows no sign of magnetic ordering and is believed to be a spin liquid [10,25].

Figure 4 shows a schematic phase diagram for some of these salts, based on the behavior of the resistivity. Chemical pressure can be set by substitution of anion molecules and modification of donor molecules. Applied pressure is simply superimposed to this chemical pressure. Overall, pressure is assumed to be roughly proportional to the inverse screened Coulomb repulsion within a dimer, so that the higher the pressure, the lower the effects of correlations. The paramagnetic insulating (PI), antiferromagnetic (AF) insulating, unconventional superconducting (SC), and metallic (M) phases are clearly realized in the phase diagram. The positions of the various compounds are determined by their ambient-pressure ground-state properties. However, the schematic phase diagram does not take the level of frustration into account, and thus does not describe the complete family, in particular κ-Cu$_2$CN$_3$. By replacing pressure by doping, the diagram looks quite similar to that of the cuprates.

Among the compounds appearing in figure 4, κ-Cl is an antiferromagnetic Mott insulator with a commensurate order at ambient pressure. The Néel temperature is around 25K and the spin moment is greater than 0.4 μ_B per dimer. By applying a pressure of about 30 MPa, it becomes a superconductor with a critical temperature of roughly 12.8K. This is a pressure-induced first-order Mott transition. The other salts appearing in the diagram behave like pressurized κ -Cl, with superconducting ground states. The SC transition temperature T_c for various members of the organic conductors decreases by decreasing the effective correlation (increasing pressure). The position of the finite-temperature metal-to-insulator transition depends on the ratio t'/t [18,19].

Table 1 shows the values of the hopping integrals

Table 1. Critical temperature (T_c) and pressure (P_c) of κ-(BEDT-TTF)$_2$X compounds.

| anion	T_c	P_c	t/t'	U/t	Ref.
κ-Cu(NCS)$_2$	10.4	0	0.84	6.8	[21]
κ-Br	11.6	0	0.68	7.2	[22]
κ-Cl	12.8	0.3	0.75	7.5	[23]
κ-Cu$_2$CN$_3$	2.8	1.5	1.06	8.2	[24]
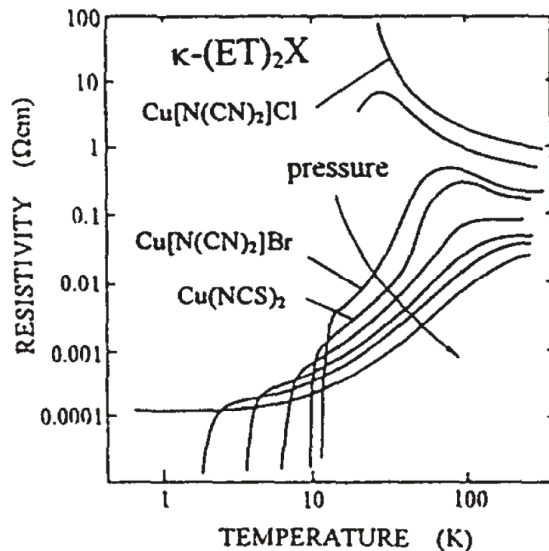
Figure 3. Resistivity profile of κ-(BEDT-TTF)$_2$X. (Reprinted from ref. [16], Copyright 1997, with permission from Elsevier.)

t/t', the SC critical temperature T_c and critical Mott transition pressure P_c, for a few well-known κ organic materials [20].

2.3. Pairing symmetry

The nature of the superconducting pairing in κ-(BEDT-TTF)$_2$X is still the object of a controversy among experimental and theoretical physicists. C-NMR measurements on κ-(BEDT-TTF)$_2$-Br show a T^3 behavior of $1/T_1$ and a Knight shift down to $0.14T_c$, which suggests an unconventional pairing with a very anisotropic gap [26]. By contrast, a fully gapped order parameter on the same salt is suggested by high-resolution specific heat measurements, because of the exponential vanishing of the electronic specific heat with T_c/T [27,28]. In another experiment, the temperature dependence of the Knight shift $k_s(T)$ below the SC-T_c suggested that the electron pair is in the spin-singlet-state; suitable candidate for this are *s*- and *d*-wave symmetries [29].

Scanning tunneling spectroscopy (STM) measurements on ET-Cu(CNS)2 show an anisotropy of the SC-gap both within the $b-c$ plane and perpendicular to it. It was concluded that the observed tunneling spectra on the plane are explained by a *d*-wave gap with nodes along the direction $\pi/4$ from k_b
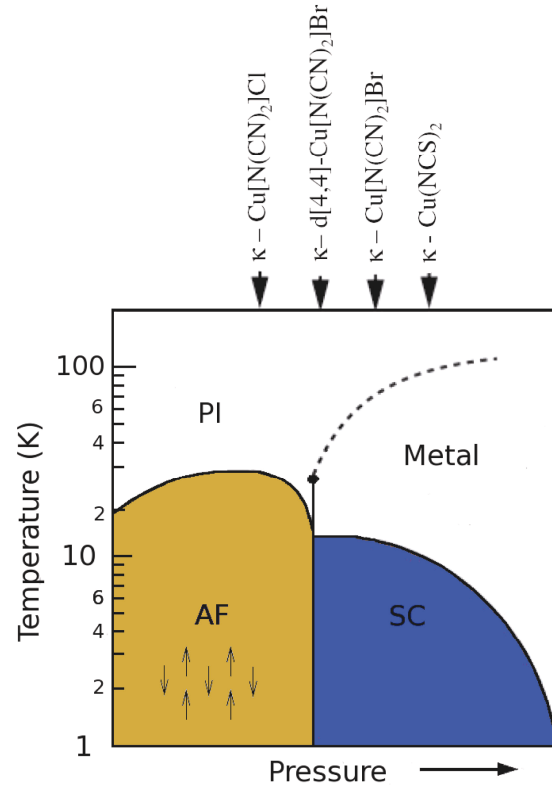
Figure 4. (color online) Generic phase diagram of κ-(BEDT-TTF)$_2$ X organic materials. The chemical or hydrostatic pressure is proportional to the inverse Coulomb interaction U. The abbreviations AF, SC, and PI stand for the antiferromagnetic, superconducting, and paramagnetic-insulator phases, respectively.

and k_c axes. These results strongly indicate that the SC pair wave function in the salt has the d_{xy}-wave symmetry [30] (with the convention for axes that we introduce below). Directional thermal conductivity measurements on κ-(BEDT-TTF)$_2$-Cu(CNS)2 showed a fourfold symmetry, with nodes at $45°$ from the k_b and k_c axes, again corresponding to a d_{xy}-wave symmetry [31]. On the other hand, ac susceptibility measurements on ET-Br lead to a mixture of *s*- and *d*-wave order parameters [32].

3. The dimer-Hubbard model

The minimum model required to study the magnetic and superconducting properties of layered organic materials is the single-band dimer-Hubbard model [33-35]. The Hamiltonian for this model can be written as

$$H = t \sum_{\langle rr' \rangle, \sigma} c_{r\sigma}^{\dagger} c_{r'\sigma} + t' \sum_{[rr'], \sigma} c_{r\sigma}^{\dagger} c_{r'\sigma} + U \sum_{r} n_{r\uparrow} n_{r\downarrow} - \mu \sum_{r,\sigma} n_{r\sigma} \ ,$$

(1)

where $c_{r\sigma}$ ($c_{r\sigma}^{\dagger}$) creates an electron (hole) at dimer site **r** on a square lattice with spin projection σ, and $n_{r\sigma} = c_{r\sigma}^{\dagger} c_{r\sigma}$ is the hole number operator. $\langle rr' \rangle$ ([rr']) indicates nearest- (next-nearest)-neighbor bonds. Here, the axes of the square lattice (x and y) correspond to nearest-neighbor bonds and are rotated by $\pi/4$ with respect to the b and c axes (see Figure 5).

In this model kinetic energy term tends to delocalize the electrons (or holes) and favors a metallic state. On the other hand, the on-site Coulomb interaction tends to localize the electrons in order to avoid doubly occupied sites and thereby favors an insulating state at half filling. Chemical or hydrostatic pressure induces a small change in the inter-dimer distance, which affects the hopping integral from dimer to dimer but not the intra-dimer Coulomb repulsion. Thus, the ratio t/U can be assimilated to pressure. The values of t' for the compounds κ-Br, κ-Cl, κ-Cu(NCS)$_2$ and κ-Cu$_2$CN$_3$ are thought to be roughly $0.5 - 0.65$, 0.75, $0.75 - 0.85$ and 1 respectively [35,10].

The dimer Hubbard model, and Hubbard-type models in general, have been treated with several theoretical methods. Many of these methods, such as slave-boson descriptions, are applied at the mean-field level are thus ignore even short-range fluctuations, which may play an important role. Because the kinetic and potential energies are most often of the same order of magnitude, perturbation theory is not practical; on the other hand, numerical methods have taken an increasingly important place. Plain exact diagonalizations are limited to small system sizes. Quantum Monte-Carlo is very useful but must be extrapolated to zero temperature and suffers from the fermion sign problem in the frustrated case [36]. Dynamical mean-field theory (DMFT) is another approximation which effectively assumes the limit of infinite spatial dimension ($D = \infty$) [37-39]. Different techniques are employed to solve the model within DMFT to study the Mott transition such as iterative perturbation theory [39-41], exact diagonalizations [42-45], renormalization group methods [46-48], and quantum Monte-carlo [49-52].

4. The variational cluster approximation

Over recent years, a few methods have been proposed that take into account short-range correlations exactly while describing the propagation of electrons over the infinite lattice. These methods are collectively called quantum cluster methods: they all involve the exact solution of the model on a finite cluster of sites, and the embedding of this cluster into an infinite lattice. They are the Dynamical Cluster Approximation (DCA)
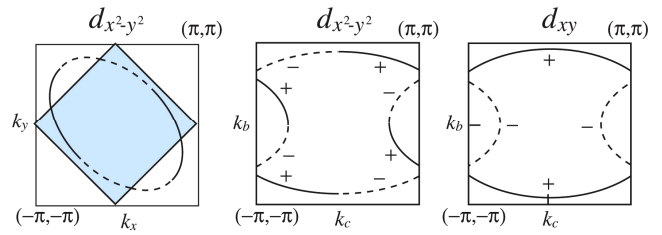
Figure 5. (color online) Left: the Fermi surface in the Brillouin zone of the dimer model, and (blue) the corresponding folded zone associated with a large unit cell containing two dimers (i.e. four molecules). The sign of the $d_{x^2-y^2}$ SC gap function is indicated by the alternating dashed and full lines. Middle: the folded Fermi surface in the reduced Brillouin zone, also rotated by $\pi/4$ (i.e. along the b and c axes). Right: same, this time indicating the signs of the d_{xy} SC gap function.

[56, 57], the Cluster Dynamical Mean Field Theory (CDMFT) [58], the Cluster Perturbation Theory (CPT) [54] and, more recently, the Variational Cluster Approximation (VCA), also called the Variational CPT (V-CPT) [11,12].

The first step of quantum cluster methods is to tile the infinite lattice of the model with identical clusters, i.e., to define a superlattice of clusters. The various cluster methods differ in the way they try to connect the properties (such as the one-particle Green function) calculated exactly with one cluster, to the corresponding property of the infinite system. Cluster Perturbation Theory is conceptually the simplest of these methods. It amounts to calculating the exact self-energy of the cluster and applying this self-energy to the whole lattice, with a proper periodization of the Green function [54, 55]. CPT includes short-range correlations on the scale of the cluster size and is also exact in both the strong and weak-coupling limits. However, it does not contain a procedure to study broken-symmetry phases (long-range order).

The VCA is an extension of CPT based on the *self-energy functional approach* (SFA) [13], and enables us to overcome this problem. This approach provides a general variational principle to use dynamical information from an exactly solvable "reference system" (here, and individual cluster) to describe the system on the infinite lattice.

The SFA defines a functional $\Omega_t[\Sigma]$ of the self-energy, which is stationary at the physical self-energy: $\delta\Omega_t[\Sigma]/\delta\Sigma = 0$. The value of the functional at the stationary point is the physical grand potential of the system. This functional can be calculated exactly, but only for a finite-dimensional space of self-energies, by defining a so-called *reference Hamiltonian H'*, which has the same interaction part as the original Hamiltonian under study, but differs from it by its one-body part, in such a way that it can be solved exactly (numerically). In the case of the VCA, the reference Hamiltonian is that of a single cluster. In terms of the exactly computed Green

function G' of the reference system (the cluster) and the non-interacting Green function G_0 of the full Hamiltonian H, the functional Ω_t reduces to a function of the one-body parameters of the reference Hamiltonian, which has the expression:

$$\Omega_t(t') = \Omega' - \int_C \frac{d\omega}{2\pi} \sum_K \ln\det\left(1 + (G_0^{-1} - G_0^{-1})G'\right), \quad (2)$$

where Ω' is the exact grand potential of the cluster. The variational principle is then applied by varying the one-body part of the cluster Hamiltonian (by varying a few parameters such as symmetry breaking Weiss fields) until the function $\Omega_t(t')$ is stationary. At this stationary point, the self-energy of the cluster is taken as the self-energy of the whole lattice, like in CPT. The value of the function Ω at this point is an approximation to the physical grand potential. We stress the nature of the approximation made here: the functional used is exact, but the space of self-energies used is restricted to the exact self-energies of a reference Hamiltonian, which is spanned by a finite number of judiciously chosen parameters. We refer to Refs [11,12] for a more detailed explanation.

5. Results and discussion

We now present the results of VCA calculations at zero temperature for the dimer Hubbard model (1) on two type of clusters: four-site (2×2) and eight-site (2×4) [17]. In order to allow for broken symmetry states, we have added Weiss fields to the cluster Hamiltonian (reference system). These symmetry-breaking terms have the following form:

$$H'_{AF} = M \sum_{\mathbf{r}} (-1)^\sigma e^{i\mathbf{Q}\cdot\mathbf{r}} n_{\mathbf{r}\sigma}, \quad (3)$$

$$H'_{SC} = \sum_{\mathbf{r},\mathbf{r}'} \left(\Delta_{\mathbf{r}\mathbf{r}'} c_{\mathbf{r}\uparrow} c_{\mathbf{r}'\downarrow} + H.c.\right), \quad (4)$$

where $\mathbf{Q} = (\pi, \pi)$ is the Néel wave vector. A nonzero value of M would induce Néel antiferromagnetism. The $d_{x^2-y^2}$ state is probed by letting $\Delta_{\mathbf{r}\mathbf{r}'} = \Delta$ if $\mathbf{r}' = \mathbf{r} \pm \mathbf{x}$ and $\Delta_{\mathbf{r}\mathbf{r}'} = -\Delta$ if $\mathbf{r}' = \mathbf{r} \pm \mathbf{y}$. On the other hand, a d_{xy} state is probed by setting

$$\Delta_{\mathbf{r},\mathbf{r}+\mathbf{x}+\mathbf{y}} = \Delta_{\mathbf{r},\mathbf{r}-\mathbf{x}-\mathbf{y}} = \Delta_1, \quad (5)$$

$$\Delta_{\mathbf{r},\mathbf{r}+\mathbf{x}-\mathbf{y}} = \Delta_{\mathbf{r},\mathbf{r}-\mathbf{x}+\mathbf{y}} = -\Delta_2. \quad (6)$$

These Weiss fields allow for the physics of long-range to seep through the cluster self-energy, but they are not part of the lattice Hamiltonian and they are determined by looking for a stationary point CPT the self-energy functional. This is not mean-field theory: the interaction term is never factorized, and the Weiss fields are not the same as the corresponding order parameters.

A word of caution about gap symmetry: the

terminology $d_{x^2-y^2}$ and d_{xy} are not rigorous in the context of the dimer model. We should instead consider the point group of the model, which is C_{2v}, and look at its irreducible representation [17,59]. C_{2v} consists of a rotation of π about the z axis, and reflections across the $\mathbf{x}+\mathbf{y}$ and $\mathbf{x}-\mathbf{y}$ lines. This group admits two possible gap symmetries for singlet superconductivity: the so-called A_2 representation, which is odd under reflections accross the $\mathbf{x}+\mathbf{y}$ and $\mathbf{x}-\mathbf{y}$ lines, and the A_1 representation, which is even. The $d_{x^2-y^2}$ state defined above corresponds to the A_2 representation, and the d_{xy} state corresponds to the A_1 representation. The C_{2v} symmetry does not require that the two lobes of the d_{xy} gap have the same size. Indeed, an s-wave gap function would also fall under this representation. Thus, the expression "extended s-wave" would be more appropriate than d_{xy}, but we nevertheless keep the latter, because it is an ingrained practice, and because the gap function does have nodes that are in the same directions as in a true d_{xy} state. Physically, the presence of nodes in an otherwise extended s-wave gap function is due to the absence of on-site pairing, because of the strong on-site Coulomb repulsion.

Besides the four variational parameters that were used and that probe broken symmetry states (M, Δ, Δ_1 and Δ_2) the chemical potential μ' on the cluster is also taken as a variational parameter to guarantee the thermodynamic consistency, which means that the electron density n should be the same whether it is calculated from the trace of the Green function ($\text{Tr}\,G$) or from the derivative of the grand potential Ω with respect to the lattice chemical potential ($-\partial\Omega/\partial\mu$).

In practice, the cluster Green function is calculated by an exact diagonalization procedure based on the band Lanczos method. The value of the functional Ω is calculated by applying eq. 2, i.e. by performing the trace with an explicit numerical integration over wavevectors and frequencies (along the imaginary axis). The values of the stationary point of the grand potential can be obtained from an optimization procedure (for instance the Newton-Raphson method) that looks for the zeros of the gradient of Ω, from initial guess values of the variational parameters. Once the stationary point is found, the other properties of the system can be derived from the calculated lattice Green function at that point, through the Dyson equation ($G^{-1} = G_0^{-1} - \Sigma(t')^{-1}$). The lattice chemical potential is adjusted so that the electron density is $n = 1$ (half-filling).

The order parameters as a function of U/t for $t'/t =$
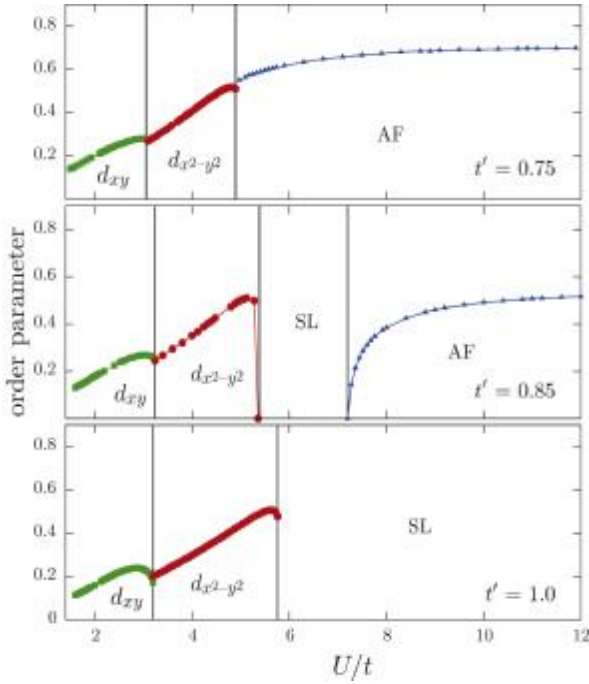
Figure 6. (color online) U/t dependence of the antiferromagnetic (blue triangles), $d_{x^2-y^2}$ (red circles, scaled by 2) and d_{xy} (green squares, scaled by 5) order parameter, obtained with the VCA on 2×2 clusters, for various values of t'/t. The vertical lines indicate the transition points, separating the various phases.

0.75, 0.85 and 1.0, are shown on figure 6 (for the 2×2 cluster) and figure 7 (for the 2×4 cluster). In the case where two solutions, for instance AF and dSC, were found, the one with the lowest value of $\Omega + \mu n$ (i.e. the lowest energy) was chosen.

We find that the system is in a Néel state when U is large enough and t' smaller than a critical value roughly equal to $0.9t$. For t' smaller than ~ 0.8, the following phases are met upon decreasing U: first an AF phase, then a SC phase with $d_{x^2-y^2}$ symmetry and finally, at low coupling, a SC phase with d_{xy} symmetry. The transitions between these phases are all of the first order, which opens the door to the possibility of macroscopic coexistence. This is indeed the case in the κ-Cl compound. For t' lying between ~ 0.8 and ~ 0.9, a paramagnetic insulating phase is intercalated between the AF and $d_{x^2-y^2}$ phases. We interpret this phase as the spin liquid phase proposed recently [10,25]. For larger values of t', the AF phase disappears, leaving the spin liquid phase dominant at strong coupling. However, we have not studied the possibility of a $120°$ magnetic order, and it may be presumed that such an order will take place around $t' = t$ for large-enough U.

The small differences between the two cluster shapes indicate that the results are not yet converged with
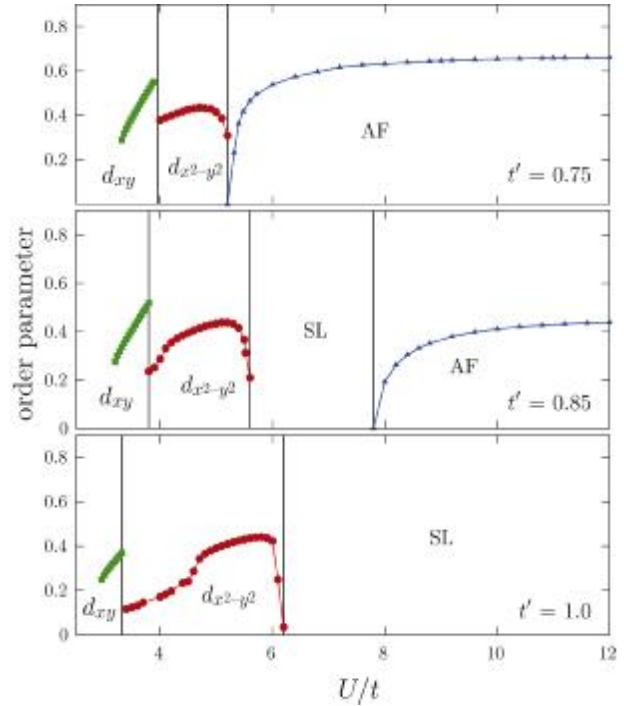

Figure 7. (color online) Same as Figure 6, this time for 2×4 clusters.

respect to cluster size. For instance, the AF order parameter is slightly smaller on the larger cluster, as it should. There are also minor differences in the values of critical parameters. But the overall picture is the same.

Figure 8 and 9 show momentum distribution curves (MDCs) for $t' = t$, and $U = 4$ and $U = 3$ respectively, obtained on an 8-site cluster. Figure 8 corresponds to a $d_{x^2-y^2}$ state. The color code indicates the spectral intensity (red is highest, purple is lowest). The gap function along the Fermi surface is indicated by the white curve, with nodes roughly at $45°$ from the axes (they are not exactly at $45°$ because of the lack of rotational symmetry of the electron dispersion relation). The AF zone boundary is indicated by the dashed line. We observe that the spectral weight is highest along the nodal directions, whereas it is depleted at the intersection of the Fermi surface with the AF zone boundary (hot spots), indicating that scattering with AF fluctuations is important, even though no long range AF order is realized in that case. Figure 9 corresponds to a d_{xy} state (at a lower value of U). The nodal directions are different, and they are close to the hot spots, which preempts the otherwise expected enhancement of the spectral intensity there. On the other hand, we notice a dip in the spectral intensity in the direction of maximal gap ($3\pi/4$ and $-\pi/4$).

We have shown that the essential physics of the layered organic superconductors can be obtained form the dimer-Hubbard model. A rigorous variational approach enables to recover the dSC and AF ground
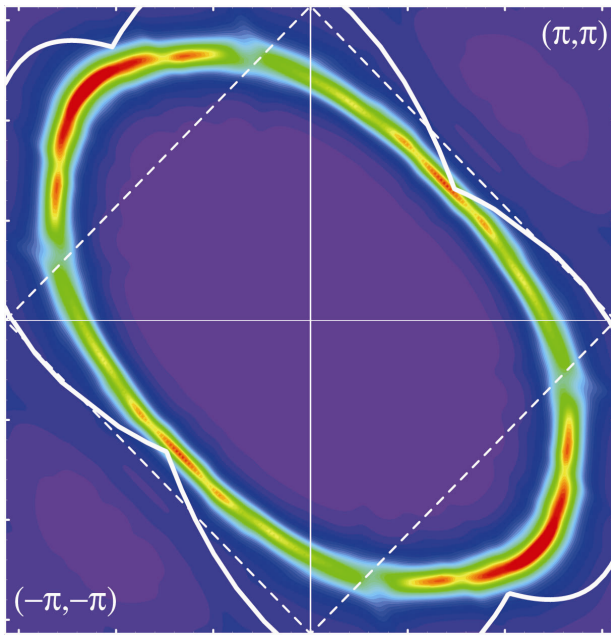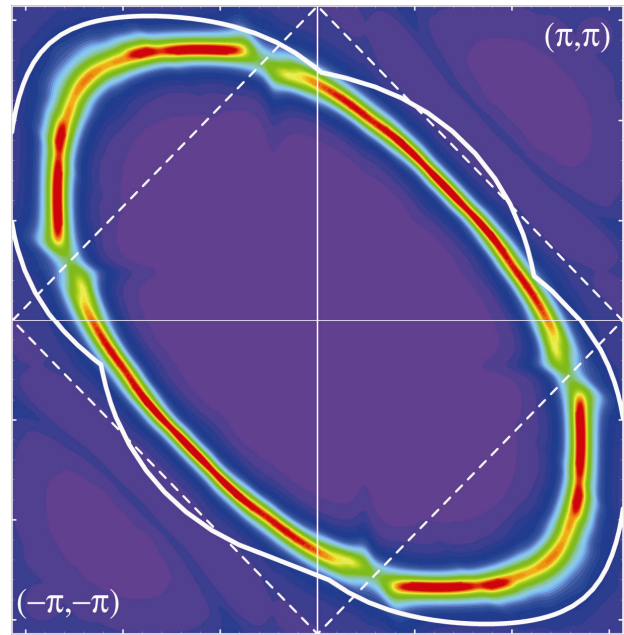
Figure 8. (color online) Momentum distribution curve, obtained from the VCA, at $t' = t$ and $U = 4t$, in a $d_{x^2-y^2}$ state. Red corresponds to the highest spectral intensity, purple to the lowest. The Fermi surface is clearly recognizable. The white curve is the SC gap function evaluated along the Fermi surface, for the value of the order parameters found at this point. The dashed lines form the AF zone boundary. The spectral intensity is depleted at the intersection of the this zone boundary with the Fermi surface. A lorentzian broadening of $\eta = 0.2t$ is used for the spectral function.

Figure 9. (color online) Same as figure 8, this time for $t' = t$ and $U = 3t$, in a d_{xy} state.

states at half filling for different values of the on-site repulsive potential. The phase transition between the phases appears to be of first order. This is consistent with the experimental results of these materials. Decreasing the potential U within the dSC region results in a transition from $d_{x^2-y^2}$ to d_{xy} pairing symmetry. The so-called spin liquid phase, without long

range order, is found for higher values of t', because of the higher level of magnetic frustration. Our calculations indicate that a pseudogap phenomenon also occurs in these systems, due to short-range AF fluctuations, even within SC phases where no AF long range order is observed.

References

1. T Ichiguro, K Yamaji and G Saito: *Organic Superconductors* (Springer, Heidelberg, 1998).
2. J Singleton, *Rep. Prog. Phys*. **63** (2000) 1111.
3. H Kino and H Fukuyama, *J. Phys. Soc. Jpn*. **64** (1995) 2726.
4. R H McKenzie, *Science* **278** (1997) 820; Comments Cond. Matt. **18** (1998) 309.
5. B J Powell, Ross H McKenzie, *cond-mat*/0607078; *cond-mat*/0607079.
6. S Tomić, M Pinterić, M Prester, D Drobac and K Maki, *Physica* C **365** (2001) 247.
7. J M Williams, *Science* **252** (1991) 1510.
8. S Lefebvre, P Wzietek, S Brown, C Bourbonnais, D Jérome. C Mézière. M Fourmigué and P Batail, *Phys. Rev. Lett*. **85** (2000) 5420.
9. T Komatsu, N Matsukawa, T Inoue and G Saito, *J Phys. Soc. Jpn*. **65** (1996) 1340.
10. Y Shimizu, K Miyagawa, K Kanoda, M Maesato and G Saito. *Phys. Rev. Lett*. **91** (2003) 107001.
11. M Potthoff, M Aichhorn and C Dahnken, *Phys. Rev. Lett*. **91** (2003) 206402.
12. C Dahnken, M Aichhorn, W Hanke, E Arrigoni and M Potthoff, *Phys. Rev*. B **70** (2004) 245110.
13. M Potthoff, Eur. *Phys. J*. B **32** (2003) 429.
14. D Sénéchal, P-L Lavertu, M-A Marois and A-M S Tremblay, *Phys. Rev. Lett*. **94** (2005) 156404.
15. M Aichhorn, E Arrigoni, M Potthoff and W Hanke, *Phys. Rev*. B **74** (2006) 024508.
16. K Kanoda, *Physica* C **282** (1997) 299.
17. P Sahebsara and D Sénéchal, *cond-mat*/0604057.
18. K Kanoda, *J. Phys. Soc. Jpn*. **75** (2006) 51007.
19. H Morita, S Watanabe and M Imada, *J. Phys. Soc. Jpn*. **71** (2002) 2109.
20. H Mori, *J. Phys. Soc. Jpn*. **75** (2006) 51003.

21. H Urayama, H Yamochi, G Saito, K Nozawa, T Sugano, M Kinoshita, S Sato, K Oshima, A Kawamoto and J Tanaka, *Chem. Lett*. **55** (1988).

22. A M Kini, U Geiser, H H Wang, K D Carlson, J M Williams, W K Kwok, K G Vandervoort, J E Thompson, D L Stupka, D Jung and M-H Whangbo, *Inorg. Chem*. **29** (1990) 2555.

23. N D Kusuch, M A Tanatar, E B Yagubskii and T Ishiguro: *JETP Lett*. **73** (2001) 429.

24. U Geiser, H H Wang, K D Carlson, J M Williams, H A Charlier, J E Heindl, G A Yaconi, B J Love, J E Schirber, D L Overmyer, J Ren and M-H Whangbo, *Inorg. Chem*. **30** (1991) 2586.

25. Y Kurosaki, Y Shimizu, K Miyagawa, K Kanoda and G Saito, *Phys. Rev. Lett*. **95** (2005) 177001.

26. H Mayaffre, P Wzietek, D Jérome, C Lenoir and P Batail, *Phys. Rev. Lett*. **75** (1995) 4122.

27. H Elsinger, J Wosnitza, S Wanka, J Hagel, D Schweitzer and W Strunz, *Phys. Rev. Lett*. **84** (2000) 6098.

28. J Müller, M Lang, R Helfrich, F Steglich and T Sasaki, *Phys. Rev*. B **65** (2002) 140509.

29. T Arai, K Ichimura, K Nomura, S Takasaki, J Yamada, S Nakatsuji, H Anzai, *Phys. Rev*. B **63** (2001) 104518.

30. K Ichimura and K Nomura, *J. Phys. Soc. Jpn*, **75** (2006) 051012.

31. K Izawa, H Yamaguchi, T Sasaki and Y Matsuda, *Phys. Rev. Lett*. **88** (2002) 27002.

32. M Pinteric, *J. Phys. IV France* **114** (2005) 245.

33. J Hubbard, *Proc. R. Soc. London* A **276** (1963) 238.

34. H Kino and H Fukuyama, *J. Phys. Soc. Jpn*. **65** (1996) 2158.

35. R McKenzie, Comm. *Cond. Mat. Phys*. **18** (1998) 309.

36. E Dagotto, *Rev. Mod. Phys*. **66** (1994) 763.

37. A Georges and G Kotliar, *Phys. Rev*. B **45** (1992) 6479.

38. M Jarrell. *Phys. Rev. Lett*. **69** (1992) 168.

39. A Georges, G Kotliar and W Krauth, *Phys. Rev. Lett*. **72** (1996) 1545.

40. A Georges and W Krauth, *Phys. Rev*. B **48** (1993) 7167.

41. M J Rozenberg, G Kotliar and X Y Zhang, *Phys. Rev*. B **49** (1994) 10181.

42. M Caffarel and W Krauth, Phys. Rev. Lett. **72** (1994) 1545.

43. M Rozenberg, G Moeller and G Kotliar, Mod. *Phys. Lett* B **8** (1994) 535.

44. Q Si, M J Rozenberg, G Kotliar and A E Ruckenstein, *Phys. Rev. Lett*. **72** (1994) 2761.

45. M P Eastwood, F Gebhard, E Kalinowski, S Nishimoto and R M Noack, *Eur. Phys. J.* B **35** (2003) 155.

46. G Moeller, Q Si, G Kotliar, M Rozenberg and D S Fisher, *Phys. Rev. Lett*. **74** (1995) 2082.

47. R Bulla, *Phys. Rev. Lett*. **83** (1999) 136.

48. R Bulla, T A Costi and D Vollhardt, *Phys. Rev*. B **64** (2001) 045103.

49. J E Hirsch and R M Fye, *Phys. Rev. Lett*. **56** (1986) 2521.

50. J Schlipf, M Jarrell, P G J van Dongen, N Blümer, S Kehrein, Th Pruschke and D Vollhardt, *Phys. Rev. Lett*. **82** (1999) 4890.

51. M J Rozenberg, R Chitra and G Kotliar, *Phys. Rev. Lett*. **83** (1999) 3498.

52. J Joo and V Oudovenko, *Phys. Rev*. B **64** (2001) 193102.

53. W Metzner, *Phys. Rev*. B **43** (1991) 8549.

54. D Sénéchal, D Perez, M Pioro-Ladriere, *Phys. Rev. Lett*. **84** (2000) 522.

55. D Sénéchal, D Perez and D Plouffe, *Phys. Rev*. B **66** (2002) 075129.

56. M H Hettler, A N Tahvildar-Zadeh, M Jarrell, T Pruschke and H Krishnamurthy, *Phys. Rev*. B **58** (1998) R7475.

57. T Maier, M Jarrell, T Pruschke and M H Hettler, *Rev. Mod. Phys*. **77** (2005) 1027.

58. G Kotliar, S Savarsov, G Pálsson and G Biroli, *Phys. Rev. Lett*. **87** (2001) 186401.

59. B J Powell, cond-mat/0603057.